coatings

MDPI

Article

Influence of MHD on Thermal Behavior of Darcy-Forchheimer Nanofluid Thin Film Flow over a Nonlinear Stretching Disc

Abdullah Dawar [1], Zahir Shah [2], Poom Kumam [3,4,5,*], Waris Khan [6] and Saeed Islam [7]

1 Department of Mathematics, Qurtuba University of Science and Information Technology, Peshawar 25000, Pakistan
2 Center of Excellence in Theoretical and Computational Science (TaCS-CoE), SCL 802 Fixed Point Laboratory, Science Laboratory Building, King Mongkut's University of Technology Thonburi (KMUTT), 126 Pracha-Uthit Road, Bang Mod, Thrung Khru, Bangkok 10140, Thailand
3 KMUTT-Fixed Point Research Laboratory, Room SCL 802 Fixed Point Laboratory, Science Laboratory Building, Department of Mathematics, Faculty of Science, King Mongkut's University of Technology Thonburi (KMUTT), 126 Pracha-Uthit Road, Bang Mod, Thrung Khru, Bangkok 10140, Thailand
4 KMUTT-Fixed Point Theory and Applications Research Group, Theoretical and Computational Science Center (TaCS), Science Laboratory Building, Faculty of Science, King Mongkut's University of Technology Thonburi (KMUTT), 126 Pracha-Uthit Road, Bang Mod, Thrung Khru, Bangkok 10140, Thailand
5 Department of Medical Research, China Medical University Hospital, China Medical University, Taichung 40402, Taiwan
6 Department of Mathematics, Kohat University of Science and technology, Kohat 26000, KP, Pakistan
7 Department of Mathematics, Abdul Wali Khan University, Mardan 23200, Pakistan
* Correspondence: poom.kum@kmutt.ac.th; Tel.: +66-2-4708-994

Received: 5 June 2019; Accepted: 9 July 2019; Published: 17 July 2019

Abstract: The aim of this research work is to increase our understanding of the exhaustion of energy in engineering and industrial fields. The study of nanofluids provides extraordinary thermal conductivity and an increased heat transmission coefficient compared to conventional fluids. These specific sorts of nanofluids are important for the succeeding generation of flow and heat transfer fluids. Therefore, the investigation of revolutionary new nanofluids has been taken up by researchers and engineers all over the world. In this article, the study of the thin layer flow of Darcy-Forchheimer nanofluid over a nonlinear radially extending disc is presented. The disc is considered as porous. The impacts of thermal radiation, magnetic field, and heat source/sink are especially focused on. The magnetic field, positive integer, porosity parameter, coefficient of inertia, and fluid layer thickness reduce the velocity profile. The Prandtl number and fluid layer thickness reduce the temperature profile. The heat source/sink, Eckert number, and thermal radiation increase the temperature profile. The suggested model is solved analytically by the homotopy analysis method (HAM). The analytical and numerical techniques are compared through graphs and tables, and have shown good agreement. The influences of embedded parameters on the flow problem are revealed through graphs and tables.

Keywords: Darcy-Forchheimer nanofluid; nonlinear extending disc; variable thin layer; HAM and numerical method

1. Introduction

Nanoparticles less than 100 nm in size suspended into a base fluid is recognized as nanofluid. Nanofluids are used in pharmaceutical procedures, microelectronics, fuel cells, hybrid powered machines, and nanotechnology fields. Choi and Eastman [1] were the first to immerse nanoparticles into a base fluid and call it a nanofluid. Through the suspension of nanoparticles, the thermophysical

properties of the conventional fluid are enhanced. The heat transmission characteristics of a nanofluid were pointed out by Wang and Mujumdar [2]. Later on, Eastman et al. [3,4] furthered this study using different base fluids. Murshed et al. [5] experimentally showed that nanofluids that contain smaller amounts of nanoparticles have higher thermal conductivities. Furthermore, increasing the volume of the nanoparticles fraction increases the thermal conductivity of the nanofluids. Maiga et al. [6] addressed the thermal and hydrodynamic behaviors of nanofluids inside a heated tube. Nanofluid flow in a circular tube with heat flux was addressed by Bianco et al. [7]. The flow processes of nanofluids inside a heated cavity were numerically addressed by Tiwari and Das [8]. The heat transmission in nanofluid flows with Brownian and thermophoresis influences was investigated by Buongiorno [9]. The heat transmission processes of nanofluids in a porous medium were examined by Kasaeian et al. [10]. The radiative MHD flow of a nanofluid experiencing a chemical reaction under the influence of thermal radiation was addressed by Ramzan et al. [11]. The impacts of Brownian motion, magnetic field, and nanoparticles volume fraction on nanofluid flow were analyzed by Sheikholeslami and Shehzad [12]. The MHD nanofluid flow over an extending surface with the influence of viscous dissipation was addressed by Besthapu et al. [13]. The heat transmission in a nanofluid flow over an oscillatory stretching sheet with radiation impacts was addressed by Dawar et al. [14]. The same nanofluid with entropy generation and magnetic field impacts was addressed by Alharbi et al. [15]. Nanofluid flow based on four different fluids in a rotating system with a Darcyian model was addressed by Shah et al. [16]. Khan et al. [17] addressed heat transmission in MHD nanofluid flow under the influence of radiation in rotating plates.Khan et al. [18] addressed nanofluid flow over a linear extending sheet under convective conditions. The viscous dissipation impact of MHD nanofluid flow with entropy generation was determined by Dawar et al. [19]. Sheikholeslami [20] examined the radiative and heat transfer in electrohydrodynamic nanofluid flow. Sheikholeslami [21] determined the MHD nanofluid flow with Brownian influence. Dawar et al. [22] addressed the flow of nanofluid over a porous extending sheet with radiation influence. Ramzan et al. [23] examined the MHD nanofluid flow using the couple stress effect. Sajid et al. [24] examined nanofluid flow over a radially extending surface. Attia et al. [25] examined the stagnation point flow in a porous medium over a radially extending surface. But and Ali [26] scrutinized the MHD flow and heat transfer with entropy generation rate over a radially stretching surface. Zeeshan et al. [27] examined ferrofluid flow over a stretching sheet under the influence of ferromagnetism, thermal radiation, and the Prandtl number. Ellahi et al. [28] addressed the impact of a magnetic field on Carreau fluid flow. Recently, the applications and development of nanofluids were discussed by Ellahi [29]. In another article, Ellahi et al. [30] addressed differential equations with application in engineering fields. The applications of heat transfer in nanofluid flows were addressed by Abu-Nada [31]. Hayat et al. [32] discussed the MHD magnetic field impact on Powell-Eyring nanomaterial flow over a nonlinear extending sheet. Hsiao [33] examined the heat convection, conduction, and mass transfer of MHD nanofluid flow over a stretching sheet. Abu-Nada [34] addressed the heat transfer in a nanofluid flow with entropy generation. Hsiao [35] analyzed the viscous dissipation and radiative influences on MHD Maxwell nanofluid flow in a thermal extrusion system. Pour and Nassab [36] examined nanofluid flows under bleeding conditions. Tian et al. [37] addressed the MHD incompressible flow of nanofluid over an extending sheet with thermophoresis and Brownian influences. Recently, Shah et al. [38] addressed the flow of nanofluid over an extending sheet with couple stress impact. Ellahi et al. [39] examined heat transmission in a boundary layer flow with MHD and entropy generation effects. Some recent study about nanofluid flow can be seen in [39–43].

In this article, a thin layer flow of Darcy-Forchheimer nanofluid over a nonlinear radially extending disc is examined. The disc is considered as porous. The homotopy analysis method (HAM) is applied to solve the nonlinear differential equations using appropriate similarities transformations. The HAM is compared with the numerical (ND-Solve) technique through graphs and tables. Section 2 confronts with the problem of formulation. In Section 3, the modeled problem is solved by HAM. In Section 4,

the impacts of embedded parameters on the fluid flow are deliberated. Section 5 presents the concluding remarks of this research.

2. Problem Formulation

The thin layer flow of a nanofluid over a nonlinear radially extending porous disc in an axially symmetric form has been assumed. The extending disc has been kept at $z = 0$. The nanofluid thickness is regulated to the thin layer with the breadth $z = h$ where h is the thin layer thickness (Figure 1). The porous disc is stretching with a nonlinear velocity $U_w = ar^n$ where n is the integer such that $n > 0$. The applied magnetic field is assumed in a vertical direction to the flow phenomena. The pressure is considered as constant. All others assumptions for the flow phenomena are used as in [24–26]. The leading equations are considered as:

$$\frac{\partial u}{\partial r} + \frac{u}{r} + \frac{\partial w}{\partial z} = 0 \tag{1}$$

$$u\frac{\partial u}{\partial r} + w\frac{\partial u}{\partial z} = \frac{\mu}{\rho}\frac{\partial^2 u}{\partial z^2} - \frac{\sigma B_0^2}{\rho}u - \frac{1}{\rho}\left(\frac{\nu}{k} + Fu\right)u \tag{2}$$

$$u\frac{\partial T}{\partial r} + w\frac{\partial T}{\partial z} = \frac{k}{\rho c_p}\frac{\partial^2 T}{\partial z^2} + \frac{\mu}{\rho c_p}\left(\frac{\partial u}{\partial z}\right)^2 - \frac{1}{\rho c_p}\frac{\partial q_r}{\partial z} + \frac{Q_0}{\rho c_p}(T_0 - T_{\text{ref}}) \tag{3}$$

Here $u, v, B_0, F = \frac{C_b}{\sqrt{Bx}}, C_b, q_r, Q_0, \rho c_p, C_b, k, \sigma, \rho, \mu$ are the components of velocity in their corresponding directions, induced magnetic strength, inertial coefficient of a permeable medium, drag coefficient, radiative heat flux, heat source/sink, effective heat capacity, thermal conductivity, kinematic viscosity, electrical conductivity, the electrical conductivity, density, and dynamic viscosity, respectively.

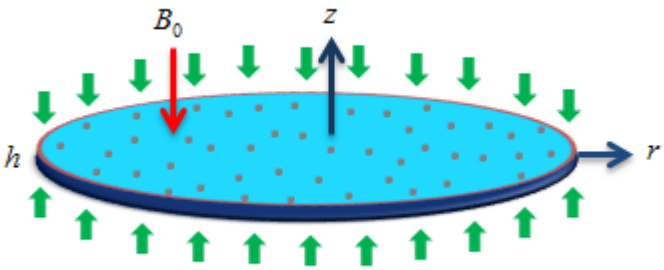

Figure 1. Geometrical illustration of the problem.

The q_r is defined as:

$$q_r = -\frac{4\sigma^*}{3k^*}\frac{\partial T^4}{\partial z} \tag{4}$$

By Taylor's expansion, T^4 can be written as:

$$T^4 = 4T_{\text{ref}}^3 T - T_{\text{ref}}^4 \tag{5}$$

In observation of Equations (4) and (5), Equation (3) is reduced as:

$$u\frac{\partial T}{\partial r} + w\frac{\partial T}{\partial z} = \frac{1}{\rho c_p}\left(k + \frac{16\sigma^* T_{\text{ref}}^3}{3k^*}\right)\frac{\partial^2 T}{\partial z^2} + \frac{\mu}{\rho c_p}\left(\frac{\partial u}{\partial z}\right)^2 + \frac{Q_0}{\rho c_p}(T_0 - T_{\text{ref}}) \tag{6}$$

The following physical conditions are defined for the nanofluid flow:

$$\begin{gathered} u = ar^n, w = 0, \theta = \theta_w \text{ at } z = 0 \\ \mu\frac{\partial u}{\partial z} = \frac{\partial \theta}{\partial z} = 0, w = \frac{udh}{dr} \text{ at } z = h \end{gathered} \tag{7}$$

The $\psi(r,z) = -\frac{r^2 U_w}{\sqrt{\mathrm{Re}}} f(\eta)$ and $\eta = \frac{z}{r}\sqrt{\mathrm{Re}}$ are developed for the similarity transformations in such a way that the components of velocity (u, w) along the radial direction and axial direction have been converted as:

$$\begin{array}{l} u = -\frac{1}{r}\frac{\partial \psi(r,z)}{\partial z} = U_w f'(\eta) \\ w = \frac{1}{r}\frac{\partial \psi(r,z)}{\partial r} = -\frac{U_w}{\sqrt{\mathrm{Re}}}\left[\left(\frac{3+n}{2}\right) f(\eta) + \left(\frac{n-1}{2}\right)\eta f'(\eta)\right] \\ T = T_0 - T_{\mathrm{ref}}\left(\frac{U_w^2}{2a\nu_f}\right)\theta(\eta) \end{array} \tag{8}$$

here, $\mathrm{Re} = \frac{rU_w}{\nu_f}$ is the Reynolds number.

The transformed velocity and temperature equations are:

$$f''' + \left(\frac{3+n}{2}\right) f f'' - n(f')^2 - Mf' - (\kappa + Frf')f' = 0 \tag{9}$$

$$(1+R)\theta'' + \mathrm{Pr}\left[\left(\frac{3+n}{2}\right) f\theta' - 2n(\theta f')\right] + Ec\mathrm{Pr}(f')^2 - \gamma\theta = 0 \tag{10}$$

with boundary conditions:

$$f(0) = 0, f'(0) = 1, \theta(0) = 1, f''(\beta) = f(\beta) = \theta\prime(\beta) = 0 \tag{11}$$

In Equations (9)–(11), $\beta = \frac{h\sqrt{\mathrm{Re}}}{r}$ represents the fluid layer thickness, $M = \frac{r\sigma B_0^2}{\rho U_w}$ indicates the magnetic field parameter, $F_r = \frac{rC_b}{U_w\sqrt{Bx}}$ represents the coefficient of inertia, $\kappa = \frac{r\nu}{kU_w}$ represents the porosity parameter, $R = \frac{16r^2\sigma^* T_{\mathrm{ref}}^3 T}{3U_w^2 kk^*}$ represents the thermal radiation parameter where σ^* is the Boltzmann constant and k^* is the coefficient of absorption, $\mathrm{Pr} = \frac{\mu c_p}{k}$ indicates the Prandtl number, $\mathrm{Ec} = \frac{U_w^2}{(c_p)\Delta T}$ represents the Eckert number, and $\gamma = \frac{r^2 Q_0}{U_w^2 \rho c_p}$ represents the heat source/sink.

The skin friction and Nusselt number are defined as:

$$\begin{array}{l} \frac{\sqrt{\mathrm{Re}}}{2} Cf = -f''(0) \\ \frac{1}{\sqrt{\mathrm{Re}}} Nu = -(1+R)\theta'(0) \end{array} \tag{12}$$

3. HAM Solution

The HAM technique is used to solve the modeled Equations (9) and (10) with the following procedure.

The primary guesses are picked as follows:

$$f_0(\eta) = \eta,\ \theta_0(\eta) = 1 \tag{13}$$

The L_f and L_θ are selected as:

$$L_f(f) = f''',\ L_\theta(\theta) = \theta'' \tag{14}$$

The resultant non-linear operators N_f and N_θ are specified as:

$$\begin{array}{c} N_f[f(\eta;\aleph)] = \frac{\mathrm{d}^3 f(\eta;\aleph)}{\mathrm{d}\eta^3} + \left(\frac{3+n}{2}\right) f(\eta;\aleph)\frac{\mathrm{d}^2 f(\eta;\aleph)}{\mathrm{d}\eta^2} - n\left(\frac{\mathrm{d}f(\eta;\aleph)}{\mathrm{d}\eta}\right)^2 \\ -M\frac{\mathrm{d}f(\eta;\aleph)}{\mathrm{d}\eta} - \left(\kappa + Fr\frac{\mathrm{d}f(\eta;\aleph)}{d\eta}\right)\frac{\mathrm{d}f(\eta;\aleph)}{d\eta} \end{array} \tag{15}$$

$$N_\theta[\theta(\eta;\aleph), f(\eta;\aleph)] = (1+R)\frac{d^2\theta(\eta;\aleph)}{d\eta^2} + \Pr\left[\begin{array}{c}\left(\frac{3+n}{2}\right)f(\eta;\aleph)\frac{d\theta(\eta;\aleph)}{d\eta} \\ -2n\left(\theta(\eta;\aleph)\frac{df(\eta;\aleph)}{d\eta}\right)\end{array}\right] + \mathrm{EcPr}\left(\frac{df(\eta;\aleph)}{d\eta}\right)^2 - \gamma\theta(\eta;\aleph) \tag{16}$$

The zeroth-order problem from Equations (9) and (10) are:

$$(1-\aleph)L_f[f(\eta;\aleph) - f_0(\eta)] = \aleph\hbar_f N_f[f(\eta;\aleph)] \tag{17}$$

$$(1-\aleph)L_\theta[\theta(\eta;\aleph) - \theta_0(\eta)] = \aleph\hbar_\theta N_\theta[\theta(\eta;\aleph), f(\eta;\aleph)] \tag{18}$$

The converted boundary conditions are:

$$\begin{gathered} f(\eta;\aleph)\big|_{\eta=0} = 0,\ \frac{df(\eta;\aleph)}{d\eta}\Big|_{\eta=0} = 1,\ \theta(\eta;\aleph)\big|_{\eta=0} = 1 \\ f(\eta;\aleph)\big|_\beta = \frac{df^2(\eta;\aleph)}{d\eta^2}\Big|_\beta = \frac{d\theta(\eta;\aleph)}{d\eta}\Big|_\beta = 0 \end{gathered} \tag{19}$$

For $\aleph = 0$ and $\aleph = 1$ we can write:

$$\begin{gathered} f(\eta;0) = f_0(\eta),\ f(\eta;1) = f(\eta) \\ \theta(\eta;0) = \theta_0(\eta),\ \theta(h;1) = \theta(\eta) \end{gathered} \tag{20}$$

When $\aleph$ fluctuates form 0 to 1, the initial solutions vary to the final solutions. Then, by Taylor's series, we have:

$$\begin{gathered} f(\eta;\aleph) = f_0(\eta) + \sum_{q=1}^{\infty} f_q(\eta)\aleph^q \\ \theta(\eta;\aleph) = \theta_0(\eta) + \sum_{q=1}^{\infty} \theta_q(\eta)\aleph^q \end{gathered} \tag{21}$$

where

$$f_q(\eta) = \frac{1}{q!}\frac{df(\eta;\aleph)}{d\eta}\Big|_{\tau=0} \text{ and } \theta_q(\eta) = \frac{1}{q!}\frac{d\theta(\eta;\aleph)}{d\eta}\Big|_{\tau=0} \tag{22}$$

The series (21) at $\aleph = 1$ converges, we obtain:

$$\begin{gathered} f(\eta) = f_0(\eta) + \sum_{q=1}^{\infty} f_q(\eta) \\ \theta(\eta) = \theta_0(\eta) + \sum_{q=1}^{\infty} \theta_q(\eta) \end{gathered} \tag{23}$$

The $q^{th}-$ order gratifies the succeeding:

$$\begin{gathered} L_f\Big[f_q(\eta) - \chi_q f_{q-1}(\eta)\Big] = \hbar_f V_q^f(\eta) \\ L_\theta\Big[\theta_q(\eta) - \chi_q\theta_{q-1}(\eta)\Big] = \hbar_\theta V_q^\theta(\eta) \end{gathered} \tag{24}$$

with boundary conditions:

$$\begin{gathered} f_q(0) = f_q'(0) = 0, \theta_q(0) = 0 \\ f_q''(\beta) = f_q(\beta) = \theta_q'(\beta) = 0 \end{gathered} \tag{25}$$

here

$$V_q^f(\eta) = f_{q-1}''' + \left(\frac{3+n}{2}\right)\sum_{k=0}^{q-1} f_{q-1-k}f_k'' - n\left(f_{q-1}'\right)^2 - Mf_{q-1}' - \left(\kappa + Frf_{q-1}'\right)f_{q-1}' \tag{26}$$

$$V_q^\theta(\eta) = (1+R)\theta_{q-1}'' + \Pr\left[\left(\frac{3+n}{2}\right)\sum_{k=0}^{q-1} f_{q-1-k}\theta_k' - 2n\left(\sum_{k=0}^{q-1}\theta_{q-1-k}f_k'\right)\right] + \mathrm{EcPr}\left(f_{q-1}'\right)^2 - \gamma\theta_{q-1} \tag{27}$$

where

$$\chi_q = \begin{cases} 0, \text{ if } \aleph \leq 1 \\ 1, \text{ if } \aleph > 1 \end{cases} \tag{28}$$

4. Results and Discussion

In this section impact of physical parameters on velocity and temperature profiles are discuses. In Figure 2, h-curve for velocity and temperature profiles are displayed. In Figures 3–7, the physical influence of the embedded parameters on the thin layer flow of Darcy-Forchheimer nanofluid over a nonlinear radially extending porous disc is presented. Figure 3 depicts the impacts of positive integer n and magnetic parameter M on $f'(\eta)$. It is determined here that both parameters show a declining behavior in the velocity profile.The nonlinearity stretching phenomena of the thin film flow reduced the thin layer with the escalation in n, because the bulky magnitude of n produced an opposing force to reduce the fluid motion. Therefore, the fluid velocity was reduced with the escalated n. Moreover, the large amount of M decreased the fluid velocity. Basically, the Lorentz force says that the resists the fluid motion on the liquid boundary which, in result, diminishes the velocity of the fluid. Figure 4 reveals the impacts of κ and F_r on $f'(\eta)$. The porous medium performed a key role during fluid flow occurrences. Significantly, the porosity parameter disturbed the boundary layer flow of liquid which, as a result, produced opposition to the fluid flow and, hereafter, a decline the velocity of the fluid. Furthermore, F_r diminished the fluid flow at the surface of the radially extending disc. This behavior occurred because the porous medium was added to the flow phenomena which decreased the coefficient of inertia, and consequently, the fluid velocity was decreased. The influence of fluid layer thickness β on $f'(\eta)$ and $\theta(\eta)$ is shown in Figure 5. Physically, the resistive force to fluid flow increased with the increase in fluid layer thickness β. The increased fluid layer thickness increased the velocity and a smaller amount of energy was needed for the motion of the fluid. Consequently, the velocity profile was reduced with an increase in fluid layer thickness. Similarly, the increase in fluid layer thickness was reduced $\theta(\eta)$. Figure 6 reveals the influences of γ and R on $\theta(\eta)$. Physically, γ acted like a heat producer which increased the boundary layer thickness and released heat to the fluid flow phenomena. Therefore, the increase in γ increased $\theta(\eta)$. The increase in R increased $\theta(\eta)$. The upsurge in R enhanced the thermal boundary layer temperature of the fluid flow; consequently, increased behaviour in $\theta(\eta)$ is observed. The impact of Pr and Ec is revealed in Figure 7. The increased Eckert number increased the temperature of the thin film flow. Actually, the Eckert number produced viscous resistance due to the presence of a dissipation term which increased the nanofluid thermal conductivity to increase the temperature field. The enhanced Prandtl number Pr reduced the temperature of the thin film flow. The higher Pr numbers (e.g.,$\Pr = 7.0$) possess lower thermal conductivity which result in a decline in temperature of the boundary layer flow. Conversely, the lower Pr numbers possess higher thermal conductivity which consequently increases the temperature of the boundary layer flow.

Figures 8 and 9 display a comparison of the homotopy analysis method (HAM) and numerical (ND-Solve) techniques $f'(\eta)$ and $\theta(\eta)$. The agreement of the HAM and numerical techniques is observed here.

The influence of entrenched parameters on Cf and Nu are displayed in Tables 1 and 2. The increasing fluid layer thickness increases the opposing force to fluid flow which, as a result, improves the Cf of the thin film flow. The escalating magnetic field increases the Cf. This influence is due to the increasing magnetic field which boosts the resistive force to the flow of fluid, called Lorentz force. The κ and Fr increase the Cf. The porosity parameter disturbs the boundary layer flow of the thin film flow which increases the resistive force to the fluid. The coefficient of inertia is directly proportional to the porosity parameter. The increase in the porosity parameter increases the coefficient of inertia which, in result, boosts the opposing force to fluid flow. The increasing positive integer boosts the nonlinearity which produces resistance to the fluid and increases the Cf. The increase in R increases the Nu. The thermal boundary layer temperature of the fluid flow increases with the increase in R which increases the heat transfer of the thin film flow. The increase in Pr increases the Nu. Usually, the large amount

of Pr reduces the nanofluid thermal conductivity. Therefore, the Nu increases with the increase in Pr. The larger amount of γ increases the Nu. This effect is due to the fact that the γ increases the boundary layer thickness of the nanofluid which, in result, increases the Nu. The increasing values of Ec reduces the Nu. The Eckert number is usually composed of the nanofluid thermal conductivity term to increase the temperature profile which, in turn, gives the opposite influence for cooling processes. The escalating positive integer increases the Nu.

Tables 3 and 4 display the assessment of the homotopy analysis method (HAM) and numerical (ND-Solve) techniques for $f'(\eta)$ and $\theta(\eta)$. The agreement of the HAM and numerical techniques is observed here.

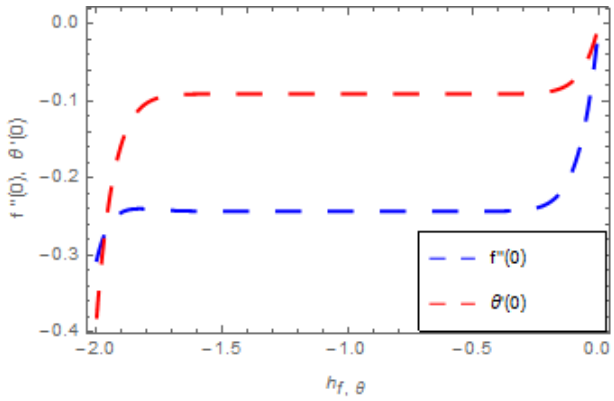

Figure 2. $\hbar$-curves for $f'(\eta)$ and $\theta(\eta)$.

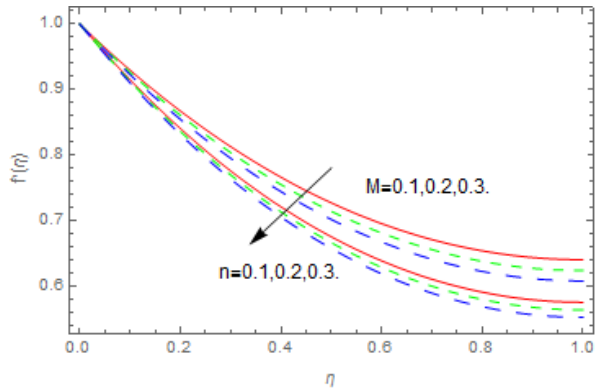

Figure 3. Impression of n and M on $f'(\eta)$.

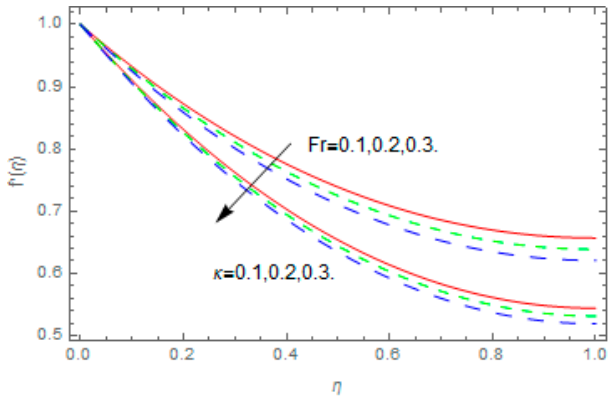

Figure 4. Impression of κ and F_r on $f'(\eta)$.

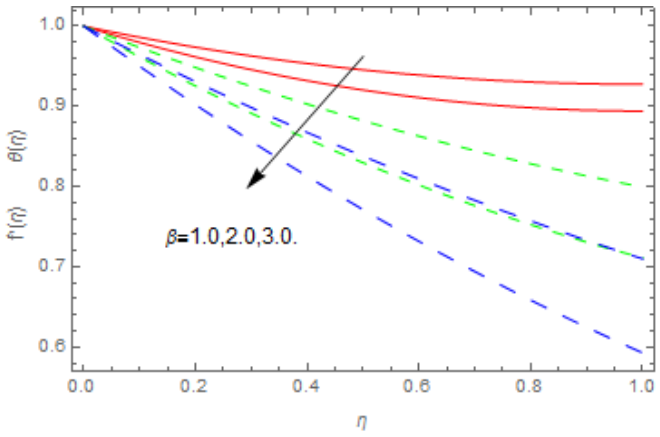

Figure 5. Impression of β on $f'(\eta)$ and $\theta(\eta)$.

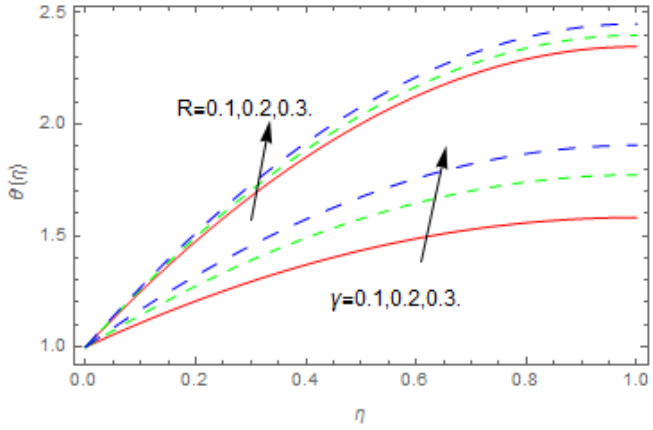

Figure 6. Impression of γ and R on $\theta(\eta)$.

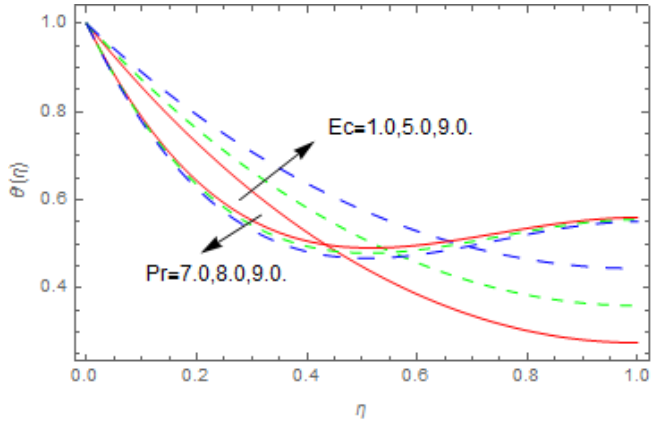

Figure 7. Impression of Pr and Ec on $\theta(\eta)$.

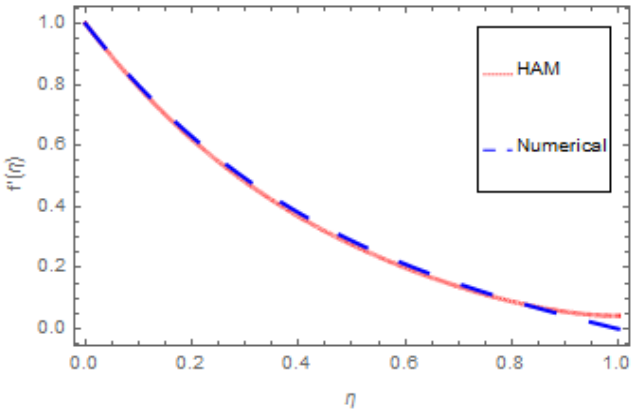

Figure 8. The assessment of HAM and ND-Solve for $f'(\eta)$.

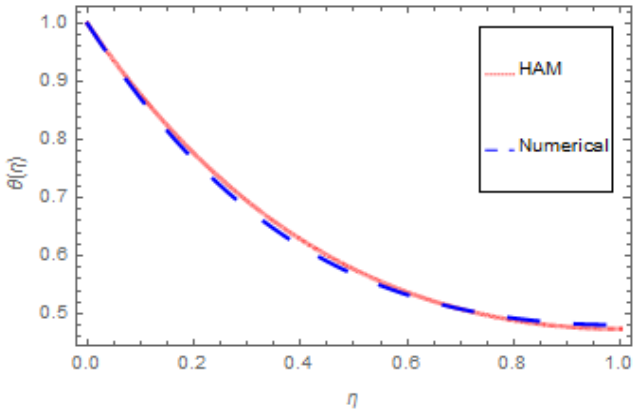

Figure 9. The assessment of HAM and ND-Solve for $\theta(\eta)$.

Table 1. The effect of embedded parameters on ***Cf*** at 15th order approximations of the homotopy analysis method (HAM).

β	*M*	κ	F_r	*n*	*Cf*
0.2	0.6	0.1	0.1	2.0	0.534624
0.3					0.761014
0.4					0.950758
	0.7				0.553042
	0.8				0.571415
	0.9				0.589744
		0.2			0.552042
		0.3			0.571415
		0.4			0.589744
			0.2		0.607370
			0.4		0.642203
			0.6		0.676780
				3.0	0.847565
				4.0	1.012080

Table 2. The effect of embedded parameters on *Nu* at 15th order approximations of the HAM.

R	Pr	γ	Ec	*n*	*Nu*
0.5	1.0	0.1	0.1	2.0	2.394070
0.6					2.553680
0.7					2.713280
	1.1				2.955850
	1.2				3.194332
	1.3				3.428861
		0.3			2.763659
		0.5			2.813816
		0.7			2.863768
			0.2		2.827741
			0.3		2.811727
			0.6		2.785875
				3.0	4.552986
				4.0	6.435682

Table 3. The assessment of the HAM and ND-Solve for $f'(\eta)$.

η	HAM	Numerical
0.0	1.000000	0.000000
0.1	0.961455	0.961589
0.2	0.945490	0.945568
0.3	0.931736	0.931656
0.4	0.920188	0.920156
0.5	0. 910827	0.910817
0.6	0.903656	0.903699
0.7	0.899547	0.899635
0.8	0.890117	0.890124
0.8	0.889466	0.883445
1.0	0.887864	0.887895

Table 4. The assessment of the HAM and ND-Solve for $\theta(\eta)$.

η	HAM	Numerical
0.0	1.000000	1.000000
0.1	0.993277	0.993900
0.2	0.986997	0.965800
0.3	0.981248	0.988250
0.4	0.976111	0.983133
0.5	0.971651	0.978612
0.6	0.967931	0.974732
0.7	0.964988	0.971530
0.8	0.962865	0.969025
0.9	0.961583	0.967233
1.0	0.961154	0.966158

5. Conclusions

The thin layer flow of Darcy-Forchheimer nanofluid over a nonlinear radially extending disc has been examined in this study. The nonlinear disc with a variable thickness of the nanofluid has been varied with the help of positive integer *n*. The magnetic field has been executed in a direction vertical to the nanofluid flow. The influences of magnetic field parameter, positive integer, porosity parameter, coefficient of inertia, fluid layer thickness, Prandtl number, heat source/sink, thermal radiation, and Eckert number on the fluid flow problem have been observed in this study. The key findings can be stated as follows:

- Increasing the magnetic field parameter, positive integer, porosity parameter, coefficient of inertia, and fluid layer thickness reduces the velocity profile.
- Increasing the Prandtl number and fluid layer thickness reduces the temperature profile.
- Increasing the heat source/sink, thermal radiation, and Eckert number increases the temperature profile.
- Increasing the fluid layer thickness, magnetic field parameter, porosity parameter, coefficient of inertia, and positive integer increases the skin friction coefficient.
- Increasing the heat source/sink, thermal radiation, Eckert number, and positive integer increases the local Nusselt number.
- Increasing the Eckert number reduces the local Nusselt number.
- An agreement between the HAM and numerical techniques is observed here.

Author Contributions: Conceptualization, A.D. and Z.S.; Methodology, A.D., Z.S. and W.K.; Software, A.D., Z.S. and S.I.; Validation, A.D. and W.K.; Resources, P.K.; Writing—Original Draft Preparation, A.D.; Writing—Review & Editing, A.D., Z.S., W.K. and S.I.; Visualization, Z.S., P.K. and S.I.

Funding: This research was funded by the Center of Excellence in Theoretical and Computational Science (TaCS-CoE), KMUTT.

Acknowledgments: This project was supported by the Theoretical and Computational Science (TaCS) Center under Computational and Applied Science for Smart Innovation Research Cluster (CLASSIC), Faculty of Science, KMUTT.

Conflicts of Interest: The author declares that they have no competing interests.

Nomenclature

a	Stretching parameter
B_0	Magnetic field (N m A^{-1})
c_P	Specific heat (J kg^{-1} K^{-1})
k	Thermal conductivity (W m^{-1} K^{-1})
n	Positive integer
Q_0	Heat flux (W m^{-2})
q_r	Radioactive heat flux (J)
u, v	Velocity components (m s^{-1})
ρ	Dynamic viscosity (MPa)
σ	Electrical conductivity (S m^{-1})
$\hbar$	Assisting parameter
Cf	Skin friction coefficient
Pr	Prandtl number
κ	Porosity parameter
β	Fluid layer thickness parameter
Ec	Eckert number
F	Permeability (m^2)
h	Thin layer thickness
k^*	Stefan Boltzmann constant
T	Fluid temperature (K)
T_{ref}	Reference temperature
Uw	Stretching velocity (m s^{-1})
η	Similarity variable
v	Kinematic viscosity (m^2 s^{-1})
σ*	Absorption coefficient
M	Magnetic field parameter
Nu	Nusselt number
R	Thermal Redation parameter
γ	Heat source/sink parameter
F_r	Coefficient of inertia parameter

References

1. Choi, S.U.S.; Estman, J.A. Enhancing thermal conductivity of fluids with nanoparticles. *ASME Publ. Fed.* **1995**, *231*, 99–106.
2. Wang, X.Q.; Mujumdar, A.S. Heat transfer characteristics of nanofluids: A review. *Int. J. Therm. Sci.* **2007**, *46*, 1–19. [CrossRef]
3. Eastman, J.A.; Phillpot, S.R.; Choi, S.U.S.; Keblinski, P. Thermal transport in nanofluids. *Annu. Rev. Mater. Res.* **2004**, *34*, 219–246. [CrossRef]
4. Eastman, J.A.; Choi, S.U.S.; Li, S.; Yu, W.; Thompson, L.J. Anomalously increased effective thermal conductivities of ethylene glycol-based nanofluids containing copper nanoparticles. *Appl. Phys. Lett.* **2001**, *78*, 718–720. [CrossRef]
5. Murshed, S.M.S.; Leong, K.C.; Yang, C. Enhanced thermal conductivity of TiO_2—Water based nanofluids. *Int. J. Therm. Sci.* **2005**, *44*, 367–373. [CrossRef]
6. Maïga, S.E.B.; Nguyen, C.T.; Galanis, N.; Roy, G. Heat transfer behaviours of nanofluids in a uniformly heated tube. *Superlattices Microstruct.* **2004**, *35*, 543–557.
7. Bianco, V.; Chiacchio, F.; Manca, O.; Nardini, S. Numerical investigation of nanofluids forced convection in circular tubes. *Appl. Therm. Eng.* **2009**, *29*, 3632–3642. [CrossRef]
8. Tiwari, R.K.; Das, M.K. Heat transfer augmentation in a two-sided lid-driven differentially heated square cavity utilizing nanofluids. *Int. J. Heat Mass Transf.* **2007**, *50*, 2002–2018. [CrossRef]
9. Buongiorno, J. Convective transport in nanofluids. *J. Heat Transf.* **2006**, *128*, 240–250. [CrossRef]
10. Kasaeian, A.; Azarian, R.D.; Mahian, O.; Kolsi, O.; Chamkha, A.J.; Wongwises, S.; Pop, I. Nanofluid flow and heat transfer in porous media: A review of the latest developments. *Int. J. Heat Mass Transf.* **2017**, *107*, 778–791. [CrossRef]
11. Ramzan, M.; Chung, J.D.; Ullah, N. Radiative magnetohydrodynamic nanofluid flow due to gyrotactic microorganisms with chemical reaction and non-linear thermal radiation. *Int. J. Mech. Sci.* **2017**, *130*, 31–40. [CrossRef]
12. Sheikholeslami, M.; Shehzad, S.A. Magnetohydrodynamic nanofluid convective flow in a porous enclosure by means of LBM. *Int. J. Heat Mass Transf.* **2017**, *113*, 796–805. [CrossRef]
13. Besthapu, P.; Haq, R.U.; Bandari, S.; Al-Mdallal, Q.M. Mixed convection flow of thermally stratified MHD nanofluid over an exponentially stretching surface with viscous dissipation effect. *J. Taiwan Inst. Chem. Eng.* **2017**, *71*, 307–314. [CrossRef]
14. Dawar, A.; Shah, Z.; Idress, M.; Khan, W.; Islam, S.; Gul, T. Impact of thermal radiation and heat source/sink on Eyring–Powell Fluid Flow over an unsteady oscillatory porous stretching surface. *Math. Comput. Appl.* **2018**, *23*, 20. [CrossRef]
15. Alharbi, S.O.; Dawar, A.; Shah, Z.; Khan, W.; Idrees, M.; Islam, S.; Khan, I. Entropy generation in MHD Eyring–Powell fluid flow over an Unsteady oscillatory porous stretching surface under the impact of thermal radiation and heat source/sink. *Appl. Sci.* **2018**, *8*, 2588. [CrossRef]
16. Shah, Z.; Dawar, A.; Islam, S.; Khan, I.; Ching, D.L.C. Darcy-Forchheimer flow of radiative carbon nanotubes with microstructure and inertial characteristics in the rotating frame. *Stud. Therm. Eng.* **2018**, *12*, 823–832. [CrossRef]
17. Khan, A.; Shah, Z.; Islam, S.; Dawar, A.; Bonyah, E.; Ullah, H.; Khan, A. Darcy-Forchheimer flow of MHD CNTs nanofluid radiative thermal behaviour and convective non uniform heat source/sink in the rotating frame with microstructure and inertial characteristics. *AIP Adv.* **2018**, *8*, 125024. [CrossRef]
18. Khan, A.S.; Nie, Y.; Shah, Z.; Dawar, A.; Khan, W.; Islam, S. Three-Dimensional nanofluid flow with heat and mass transfer analysis over a linear stretching surface with convective boundary conditions. *Appl. Sci.* **2018**, *8*, 2244. [CrossRef]
19. Dawar, A.; Shah, Z.; Khan, W.; Idrees, M.; Islam, S. Unsteady squeezing flow of magnetohydrodynamic carbon nanotube nanofluid in rotating channels with entropy generation and viscous dissipation. *Adv. Mech. Eng.* **2019**, *11*, 1–18. [CrossRef]
20. Sheikholeslami, M. Numerical investigation of nanofluid free convection under the influence of electric field in a porous enclosure. *J. Mol. Liq.* **2018**, *249*, 1212–1221. [CrossRef]
21. Sheikholeslami, M. CuO-water nanofluid flow due to magnetic field inside a porous media considering Brownian motion. *J. Mol. Liq.* **2018**, *249*, 921–929. [CrossRef]

22. Dawar, A.; Shah, Z.; Khan, W.; Islam, S.; Idrees, M. An optimal analysis for Darcy-Forchheimer 3-D Williamson nanofluid flow over a stretching surface with convective conditions. *Adv. Mech. Eng.* **2019**, *11*, 1–15. [CrossRef]
23. Ramzan, M.; Sheikholeslami, M.; Saeed, M.; Chung, J.D. On the convective heat and zero nanoparticle mass flux conditions in the flow of 3D MHD Couple Stress nanofluid over an exponentially stretched surface. *Sci. Rep.* **2019**, *9*, 562. [CrossRef] [PubMed]
24. Sajid, M.; Hayat, T.; Asghar, S. Non-similar solution for the axisymmetric flow of a third-grade fluid over a radially stretching sheet. *Acta Mech.* **2007**, *189*, 193–205. [CrossRef]
25. Attia, H.A.; Ewis, K.M.; Abdeen, M.A.M. Stagnation point flow through a porous medium towards a radially stretching sheet in the presence of uniform suction or injection and heat generation. *J. Fluids Eng.* **2012**, *134*, 081202. [CrossRef]
26. But, A.S.; Ali, A. Effects of Magnetic Field on entropy generation in flow and heat transfer due to a radially stretching surface. *Phys. Lett.* **2013**, *30*, 024701. [CrossRef]
27. Zeeshan, A.; Majeed, A.; Ellahi, R. Effect of magnetic dipole on viscous ferro-fluid past a stretching surface with thermal radiation. *J. Mol. Liq.* **2016**, *215*, 215–549. [CrossRef]
28. Ellahi, R.; Mubeshir Bhatti, M.; Khalique, C.M. Three-dimensional flow analysis of Carreau fluid model induced by peristaltic wave in the presence of magnetic field. *J. Mol. Liq.* **2017**, *241*, 1059–1068. [CrossRef]
29. Ellahi, R. Special Issue on recent developments of nanofluids. *Appl. Sci.* **2018**, *8*, 192. [CrossRef]
30. Ellahi, R.; Fetecau, C.; Sheikholeslami, M. Recent advances in the application of differential equations in mechanical engineering problems. *Math. Probl. Eng.* **2018**, *2018*, 1584930. [CrossRef]
31. Abu-Nada, E. Application of nanofluids for heat transfer enhancement of separated flows encountered in a backward facing step. *Int. J. Heat Fluid Flow* **2008**, *29*, 242–249. [CrossRef]
32. Hayat, T.; Sajjad, R.; Muhammad, T.; Alsaedi, A.; Ellahi, R. On MHD nonlinear stretching flow of Powell—Eyring nanomaterial. *Results Phys.* **2017**, *7*, 535–543. [CrossRef]
33. Hsiao, K.-L. Stagnation electrical MHD nanofluid mixed convection with slip boundary on a stretching sheet. *Appl. Therm. Eng.* **2016**, *98*, 850–886. [CrossRef]
34. Abu-Nada, E. The present research investigates second law analysis of laminar flow over a backward facing step (BFS). Entropy generation due to separation, reattachment, recirculation and heat transfer is studied numerically. *Entropy* **2005**, *7*, 234–252. [CrossRef]
35. Hsiao, K.-L. Combined electrical MHD heat transfer thermal extrusion system using Maxwell fluid with radiative and viscous dissipation effects. *Appl. Therm. Eng.* **2017**, *112*, 1281–1288. [CrossRef]
36. Pour, M.; Nassab, S. Numerical investigation of forced laminar convection flow of nanofluids over a backward facing step under bleeding condition. *J. Mech.* **2012**, *28*, N7–N12. [CrossRef]
37. Tian, X.-Y.; Li, B.W.; Hu, Z.-M. Convective stagnation point flow of a MHD non-Newtonian nanofluid towards a stretching plate. *Int. J. Heat Mass Transf.* **2018**, *127*, 768–780. [CrossRef]
38. Shah, Z.; Dawar, A.; Alzahrani, E.; Kumam, P.; Khan, A.J.; Islam, S. Hall Effect on couple stress 3D nanofluid flow over an exponentially stretched surface with Cattaneo Christov heat flux model. *IEEE Access* **2019**, *7*, 64844–64855. [CrossRef]
39. Ellahi, R.; Alamri, S.Z.; Basit, A.; Majeed, A. Effects of MHD and slip on heat transfer boundary layer flow over a moving plate based on specific entropy generation. *J. Taibah Univ. Sci.* **2018**, *12*, 476–482. [CrossRef]
40. Khan, A.S.; Nie, Y.; Shah, Z. Impact of thermal radiation on magnetohydrodynamic unsteady thin film flow of Sisko fluid over a stretching surface. *Processes* **2019**, *7*, 369. [CrossRef]
41. Ullah, A.; Alzahrani, E.O.; Shah, Z.; Ayaz, M.; Islam, S. Nanofluids thin film flow of Reiner-Philippoff fluid over an unstable stretching surface with brownian motion and thermophoresis effects. *Coatings* **2019**, *9*, 21. [CrossRef]
42. Alsagri, A.S.; Nasir, S.; Gul, T.; Islam, S.; Nisar, K.S.; Shah, Z.; Khan, I. MHD thin film flow and thermal analysis of blood with CNTs nanofluid. *Coatings* **2019**, *9*, 175. [CrossRef]
43. Saeed, A.; Shah, Z.; Islam, S.; Jawad, M.; Ullah, A.; Gul, T.; Kumam, P. Three-dimensional casson nanofluid thin film flow over an inclined rotating disk with the impact of heat generation/consumption and thermal radiation. *Coatings* **2019**, *9*, 248. [CrossRef]

© 2019 by the authors. Licensee MDPI, Basel, Switzerland. This article is an open access article distributed under the terms and conditions of the Creative Commons Attribution (CC BY) license (http://creativecommons.org/licenses/by/4.0/).